Aerospace Science and Technology 38 (2014) 56–63

Contents lists available at ScienceDirect

Aerospace Science and Technology

www.elsevier.com/locate/aescte

Numerical study of the aerodynamics of a NACA 4412 airfoil in dynamic ground effect

Qiulin Qu [a], Xi Jia [a], Wei Wang [a], Peiqing Liu [a], Ramesh K. Agarwal [b,*]

[a] Beijing University of Aeronautics and Astronautics, Beijing, 100191, China
[b] Washington University in St. Louis, St. Louis, MO 63130, USA

ARTICLE INFO

Article history:
Received 24 October 2013
Received in revised form 18 May 2014
Accepted 30 July 2014
Available online 8 August 2014

Keywords:
Dynamic ground effect
Compression work
Downwash flow
Incidence effect

ABSTRACT

The distance between an airplane and the ground keeps constantly changing during take-off and landing. Thus, the aerodynamics is influenced by the dynamic ground effect (DGE). In this paper, the landing process of a NACA 4412 airfoil is simulated numerically to investigate the influence of DGE. Several sink rates are imposed on the airfoil. Analyses of the results show that DGE can be divided into three regions based on the aerodynamics and flow physics which depend upon the ride height above the ground. In the large height region, the lift in DGE does not change with decrease in height and is equal to the lift in static ground effect (SGE) with the same angle of attack. Ground effect is insignificant and the physics that governs the flow is due to the incidence effect induced by the sinking movement. In the medium height region, the lift in DGE increases with decreasing height and is almost equal to the lift in SGE with the same angle of attack. Both SGE and the incidence effect due to sinking govern the flow field. In the small height region, the lift in DGE increases rapidly with decreasing height and is significantly larger than that in SGE with the same angle of attack. Furthermore in this region, in addition to SGE and incidence effect, the compression work effect becomes very important. At relatively small height, the air below the airfoil does not have sufficient space to escape due to the blockage from the ground as the airfoil moves downwards towards the ground. Therefore this air gets compressed and its pressure increases which enhances the lift. This is the so-called compression work effect.

1. Introduction

The flow around an aircraft is forced to be parallel to the ground due to ground effect when the aircraft flies in the proximity to the ground. Thus, the aerodynamics in ground effect is significantly different from those out of the ground effect [15,19].

In the realm of ground effect aerodynamics, majority of previous investigations have focused on steady flow around airfoils [1,6,8,17], wings [7,20] and aircrafts [12,18] at fixed ride heights above the ground. Examining the flow physics and its contribution to the aerodynamic forces and moments, static ground effect (SGE) aerodynamics can be classified into three categories: (1) chord dominated and (2) span dominated ground effect of high aspect ratio wings [16] and (3) ground effect of delta wings [14].

During take-off and landing, an aircraft respectively moves away or towards the ground and its height above the ground changes continuously with time; thus the air flow around it is unsteady. In the past, majority of investigators have treated the dynamic ground effect (DGE) as quasi-steady, but recent studies [9,10] indicate that the unsteady flow can be considered as quasi-steady only when the sink or climbing rates are very small. However, the sink rate is usually large during emergency landing. Therefore, the study of DGE at higher sink rates is of considerable interest to ensure flight safety during take-off and landing.

Previous DGE studies have focused on flight and wind tunnel tests of delta wings. Cord et al. [4] studied experimentally the DGE of an F-15 fighter aircraft and found that the lift increment in DGE is smaller than that in SGE, and the difference enhances with the decreasing sink rate. Curry [5] presented the experimental data for F-16XL during landing process and arrived at the similar conclusion. He also introduced an engineering calculation method for DGE. Baker et al. [2] have also claimed by conducting flight tests that the aerodynamics of aircrafts in ground effect has close relationship with sink rate. A delta wing typically has detached flow; therefore its flow behavior in DGE and the generated aerodynamic forces cannot be extrapolated to understand the behavior of a high aspect ratio wing in DGE which typically has attached flow. Furthermore even today, the flow physics of a delta wing in DGE is not completely understood.

* Corresponding author, the William Palm Professor of Engineering in the Department of Mechanical Engineering & Materials Science. Tel.: +1 314 935 6091.
E-mail address: agarwalr@seas.wustl.edu (R.K. Agarwal).

http://dx.doi.org/10.1016/j.ast.2014.07.016
1270-9638/

Table 1
Parameters used in the numerical simulation.

SGE	
Angle of attack α (°)	0, 2, 4, 6, 8, 10
Non-dimensionalized ride height h/c	1.00, 0.80, 0.60, 0.40, 0.30, 0.20, 0.15, 0.10, 0.05
DGE	
Pitch angle θ (°)	2, 4, 6, 8
Sink velocity V_s (m/s)	1.075, 2.154, 3.237
Flight path angle γ (°)	−2, −4, −6

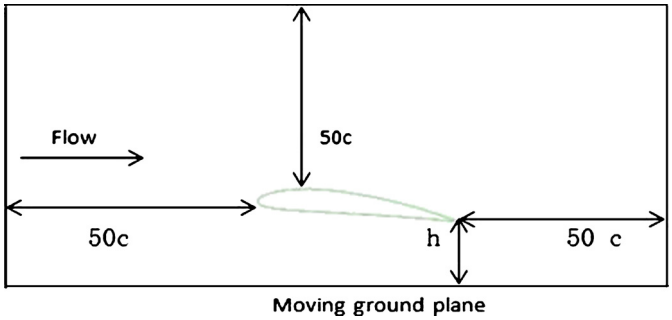

Fig. 1. Sketch of the computational domain for SGE simulation.

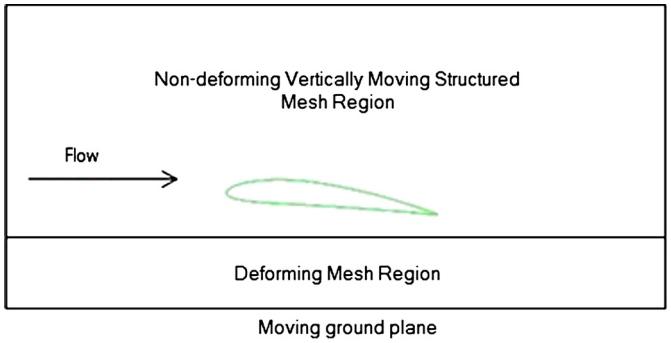

Fig. 2. Sketch of the computational domain for DGE simulation.

Regarding chord dominated DGE, Chen and Schweikhard [3] and Nuhait and Zedan [11] studied a 2D flat plate moving towards the ground using vortex-lattice method. Chen and Schweikhard assumed that the wake was straight along the flight path, while Nuhait and Zedan allowed the wake to deform freely. Both studies have indicated that the lift in DGE is larger than that in SGE, and the difference becomes larger with larger sink rate. Qu et al. [13] simulated the landing process of a NACA 4412 airfoil with the pitch angle of 4° and the flight path angle of −4° using finite volume method. They also found the lift in DGE is larger than that in SGE, and introduced the compression work concept to explain the lift enhancement phenomenon of DGE. Matsuzaki et al. [9] conducted a wind tunnel test of a NACA 6412M airfoil in DGE using a fixed ground plane. The airfoil was set to move perpendicular to the oncoming stream upwards as well as downwards at a constant velocity. Results showed that, compared with the steady case at the same height and angle of attack, the lift in the sinking case was smaller. Contrary results were found in climb. The conclusion of Ref. [9] is contrary to that in Refs. [3,11,13] which may be due to the fixed ground plane used in the experiment of Ref. [9]. Molina and Zhang [10] investigated numerically the aerodynamic characteristics of an inverted airfoil close to the ground with sinusoidal vertical movement perpendicular to a uniform free-stream. However, they focused on the phenomenon that the peak of the aerodynamic forces lags behind the minimum ride height, and did not discuss the unsteady flow and the magnitudes of lift and drag forces.

This paper is a continuation of the work reported in Ref. [13]. This paper extends the pitch angle range and the sink rate range to obtain more general aerodynamic characteristics of DGE.

2. Numerical method and mesh

In the present simulation, the airfoil is NACA 4412, the free-stream velocity is set at 30.8 m/s, and Reynolds number based on chord length is 3×10^5. Other parameters are shown in Table 1. The definition of ride height h is shown in Fig. 1.

Formula for angle of attack in dynamic effect is given by:

$$\alpha = \theta - \gamma \tag{1}$$

In the SGE simulation, since the velocity of the airfoil only has a horizontal component, the airfoil is set at stationary condition. The ground and the inlet airflow velocities are set at a constant speed which is equal to the airfoil velocity but is in the opposite direction. In DGE simulation, the velocity of the airfoil has a horizontal component as well as a vertical component. The ground and the inlet boundary conditions are the same as those in SGE. The airfoil moves towards the ground at the vertical velocity component; and the relative movement between the airfoil and the ground is accomplished by using the dynamic mesh method.

In the SGE simulation, a quadrilateral computational domain is used (Fig. 1). The inlet, outlet and upper boundaries of the computational domain are all positioned away from the airfoil at a distance of 50c. The distance from the ground to the trailing edge of the airfoil is the ride height h. The ground boundary condition is set as no slip moving wall; for the inlet, outlet and upper boundaries, far-field pressure boundary condition is employed. A multi-block structured mesh is employed.

The computational domain in DGE is the same as that in SGE, but is divided into two blocks (Fig. 2). Both blocks have structured grid. The upper block descends with the airfoil at a vertical velocity component to ensure that the mesh around the airfoil does not deform. The cells in the lower block deform in the manner of dynamic layering. To compare the results with the cases in SGE at different ride heights, the airfoil in DGE descends from $h/c = 2$ to $h/c = 0.046$; corresponding cell number range is from 400,000 to 200,000.

SGE simulation is conducted by solving the steady compressible Reynolds-Averaged Navier–Stokes (RANS) equations, while DGE simulation is conducted by solving the unsteady compressible RANS equations. Turbulent flow is modeled with the Spalart–Allmaras (S–A) model. The equations are solved using the finite-volume solver in ANSYS FLUENT; convection terms and diffusion terms are discretized with second-order upwind scheme and central difference scheme respectively. The unsteady term is discretized with first-order implicit scheme. SIMPLEC algorithm is adopted to calculate the velocity and pressure. Fig. 3 shows a typical block-structured mesh around the airfoil in DGE.

3. Numerical method validation

Tyrrell-026 airfoil is chosen to validate the numerical method's accuracy for predicting the aerodynamic forces of an airfoil in

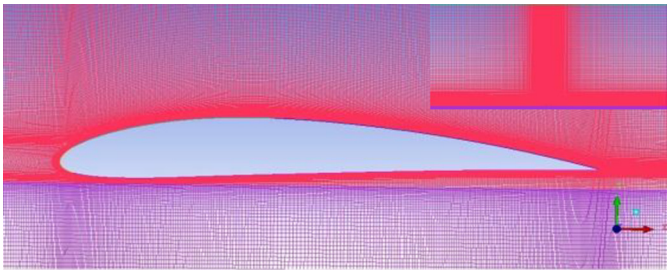

Fig. 3. Block-structured mesh around the NACA 4412 airfoil in DGE.

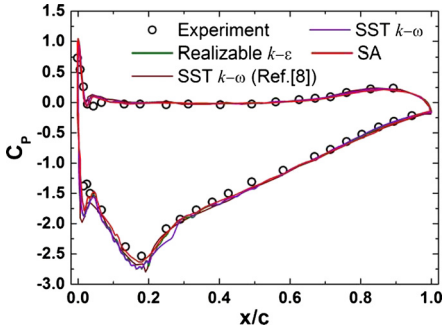

Fig. 4. Comparison of computed and experimental pressure coefficient for Tyrrell-026 airfoil.

ground effect. This simulation is intended to reproduce the wind tunnel data reported in Ref. [8]. The test conditions were: the ride height $h/c = 0.224$, the angle of attack $\alpha = 3.6°$, the free-stream velocity $V_\infty = 30$ m/s and $\mathrm{Re} = 4.6 \times 10^5$ based on the chord length; the ground is simulated as a moving belt. For this case, aerodynamic forces and surface pressures were measured in a wind tunnel test. Doig and Barber [6] simulated the aerodynamics of both a 2D airfoil and a 3D wing in SGE using three turbulence models: the SA, realizable k–ε, and shear stress transport (SST) k–ω models; the numerical simulation of the 3D case completely reproduced the results from the wind tunnel test in Ref. [8]. Results showed that although endplates were installed on the wing in the experiment, the 3D effects could not be eliminated on the wingtip. As a result, the down-force coefficient of the wing measured by force balance is smaller than that of a 2D airfoil. At the same time, the three turbulence models showed similar accuracy level in predicting the surface pressure.

The settings of the computational domain, mesh layout, boundary conditions and numerical method used for this Tyrrell-026 airfoil are kept the same as those used in our NACA 4412 SGE simulation (described in Section 2). The number of cells is 200,000. The SA, realizable k–ε, and SST k–ω models are compared to decide the most applicable turbulence model for the GE simulation. Mahon and Zhang [8] investigated six turbulence models and concluded that no single turbulence model can predict the surface pressure accurately for all ride heights, but the SST k–ω model gave the most accurate prediction for this ride height. Fig. 4 shows the pressure coefficient computed from our CFD simulation and its comparison with the experimental and CFD data from Mahon and Zhang. Except for the suction peak region on the lower surface, the three turbulence models produced a similar pressure distribution which matched the experimental data quite well. As to the suction peak, the realizable k–ε and SST k–ω models both overestimate it, but the SA model shows a good agreement with the experimental data (this is the reason that the SA model is used in our NACA 4412 simulations). The down-force coefficient in the experimental data is reported to be 1.286, our computed value from the SA model is 1.371; the relative error is 6.2%. These results demonstrate the high accuracy of our numerical simulation.

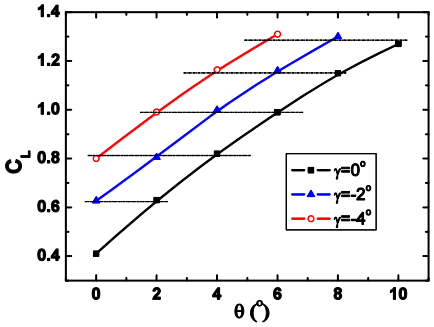

Fig. 5. Lift coefficients of NACA 4412 airfoil at different sink rates in an unbounded flow field.

Grid independence of the solutions is assessed by constructing a new grid with additional refinement. Consider the case with $\alpha = 6°$ and $h/c = 0.1$ as an example. With the same computational domain and mesh layout, the number of cells in the fine grid is roughly 1.5 times those in the original grid (197,210 cells). The cell height in the first layer in the refined and original grid is $0.5 \times 10^{-5}c$ and $1 \times 10^{-5}c$ respectively. The lift coefficient C_L of the fine mesh exceeds that of the original mesh by 1.49%, which is acceptable. Therefore in the following simulations, the original grid is adopted in order to save computing resources without compromising accuracy.

For DGE simulation, the airfoil descends impulsively towards the ground and therefore an additional vertical spatial distance is needed to obtain stable convergent solutions for C_L and C_D. To obtain the spatial distance, the cases with $\theta = 4°$ and $\gamma = -2°$, $-4°$ and $-6°$ are simulated. Results show that C_L becomes stable when the airfoil descends for about $0.6c$ from its starting point of descent. As a result, it is feasible to descend from $h/c = 2$ in DGE simulation.

4. Results and discussion

4.1. Lift behavior

From the intuitive viewpoint, DGE is the coupling of SGE and the dynamic effect due to sinking.

Considering dynamic effect in an unbounded flow field, i.e. the airfoil descends perpendicularly to the free-stream, the C_L at different sink rates is plotted in Fig. 5. It can be seen that C_L vs. θ curves for $\gamma = -2°$ and $-4°$ are similar and parallel to the static C_L vs. θ curve ($\gamma = 0°$) with lateral displacement of 2° and 4° to the left respectively. Thus the lift of the descending airfoil is equal to that of a static airfoil with a same angle of attack. Therefore, dynamic effect can be explained by the airfoil incidence effect in an unbounded flow field.

Figs. 6 and 7 show the variation of C_L with ride height h/c at different sink rates. The lifts in both SGE and DGE increase as h/c decreases (except for the case with $\alpha = \theta - \gamma = 0°$ in SGE, in which the lift decreases as h/c decreases). This is because of the Venturi channel that forms between the ground and the lower surface of the airfoil. In this channel, the airflow is accelerated and its pressure is reduced, resulting in a decrease in the lift. This phenomenon becomes more apparent with decreasing h/c, which is similar to the case of inverted race-car airfoil in negative ground effect. This aspect is beyond the scope of this paper.

As can be seen from Figs. 6 and 7, for $h/ \geq 0.5$, C_L in DGE is almost equal to C_L in SGE for the same angle of attack. When h/c is below 0.5, C_L in DGE is larger than that in SGE and the difference between the two becomes larger with the decrease in h/c and the increase in sink rate. For example, at $\theta = 4°$ and

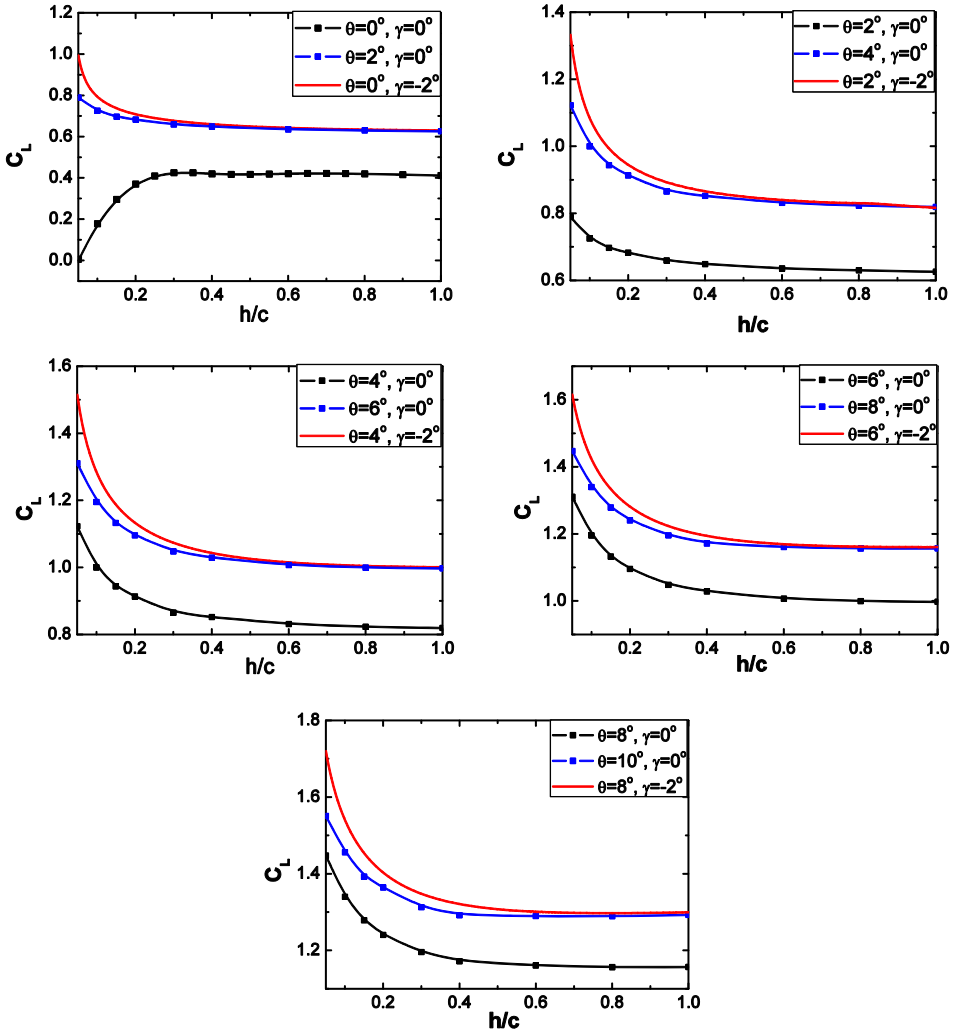

Fig. 6. Variation of lift coefficient with ride height for various values of θ and at $\gamma = 0$ and $-2°$.

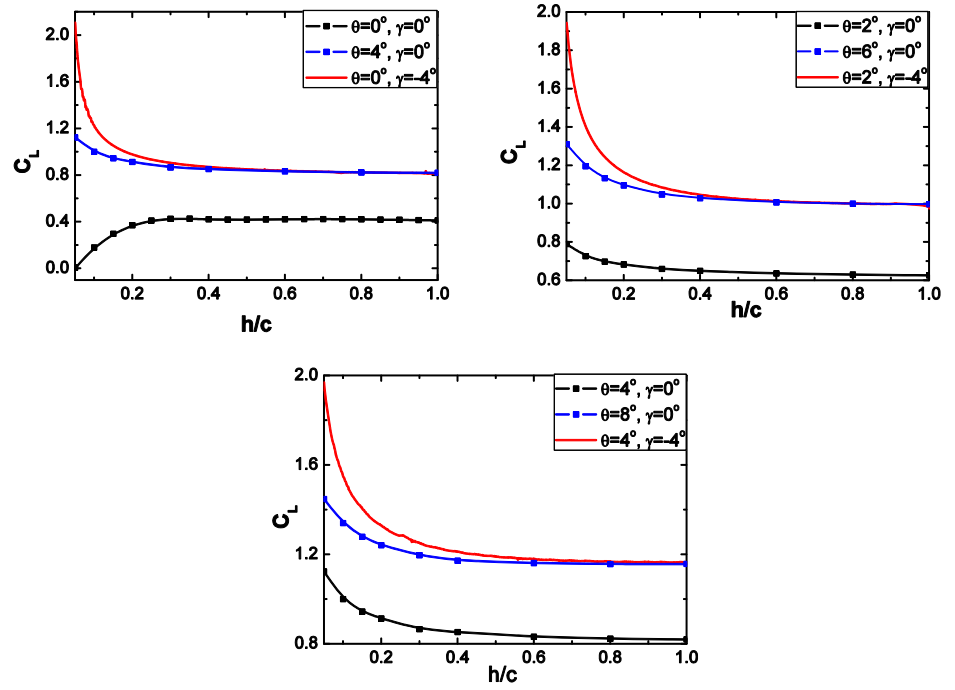

Fig. 7. Variation of lift coefficient with ride height for various values of θ and $\gamma = 0$ and $-4°$.

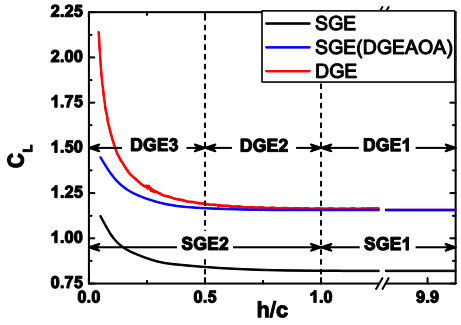

Fig. 8. SGE and DGE regions defining the variation of lift curve with ride height: SGE (DGEAOA) presents the lift curve of SGE with the same angle of attack as DGE.

$h/c = 0.05$, $\Delta C_L = 0.2$ for $\gamma = -2°$; $\Delta C_L = 0.503$ for $\gamma = -4°$; and $\Delta C_L = 0.85$ for $\gamma = -6°$ where

$$\Delta C_L = C_{L,h,\alpha,\gamma} - C_{L,h,\alpha} \tag{2}$$

In Eq. (2), $C_{L,h,\alpha,\gamma}$ refers to the lift coefficient in DGE with ride height h, angle of attack α and flight path angle γ, and $C_{L,h,\alpha}$ refers to the lift coefficient in SGE with ride height h and angle of attack α.

Examining the characteristics of C_L vs. h/c curves in DGE discussed above and considering the results of the previous work in SGE, the relationship between the lift coefficient and ride height in chord dominated ground effect can be described as follows (see Fig. 8).

For SGE, there is a critical ride height $h/c = 1.0$, which divides the C_L curve into two regions (it can be noted from previous work on SGE):

1) SGE 1: $h/c > 1.0$, lift remains constant regardless of the changes in h/c; this is the no-ground effect region.
2) SGE 2: $h/c < 1.0$, lift increases with the decrease in h/c; this is the SGE region.

For DGE, there exist two critical heights, one is $h/c = 1.0$ and the other is $h/c \approx 0.5$ which divide the C_L curve into three regions:

1) DGE 1: $h/c > 1.0$, lift in DGE remains unchanged with decrease in h/c and is the same as that in SGE for the same angle of attack. The major physics that governs the flow in this region is due to the incidence effect.
2) DGE 2: $0.5 < h/c < 1.0$, lift in DGE increases with decrease in h/c, and is nearly the same as that in SGE for the same angle of attack (the former is slightly larger). The main physics governing the flow is due to both SGE and incidence effect.
3) DGE 3: $h/c < 0.5$, lift in DGE increases dramatically with the decrease in h/c, and is much larger than that in SGE for the same angle of attack. As h/c decreases, this difference becomes more significant. Three physical factors control the flow: SGE, the incidence effect and the compression work effect (it is described below).

From the above discussion, we can conclude that when the sink rate is small, DGE can be considered as quasi-steady SGE. Furthermore when the sink rate increases (the largest sink rate in this paper is corresponding to $\gamma = -6°$), as long as $h/c > 0.5$, DGE can still be treated as quasi-steady SGE with high accuracy.

4.2. Pressure distribution

The pressure coefficients of NACA 4412 with $\theta = 4°$ at different h/c and γ are shown in Fig. 9. The pressure coefficient is defined by the equation:

$$C_p = \frac{p - p_\infty}{\frac{1}{2}\rho V_\infty^2} \tag{3}$$

As the airfoil moves closer to the ground, C_p increases dramatically on the high pressure surface of the airfoil. $C_p > 1$ is observed on almost the entire lower surface of the airfoil at small h/c (see Fig. 9c) and Fig. 9d)); the suction peak exhibits an increase while suction decreases slightly on other parts of the suction surface resulting in a larger adverse pressure gradient. Another aspect to

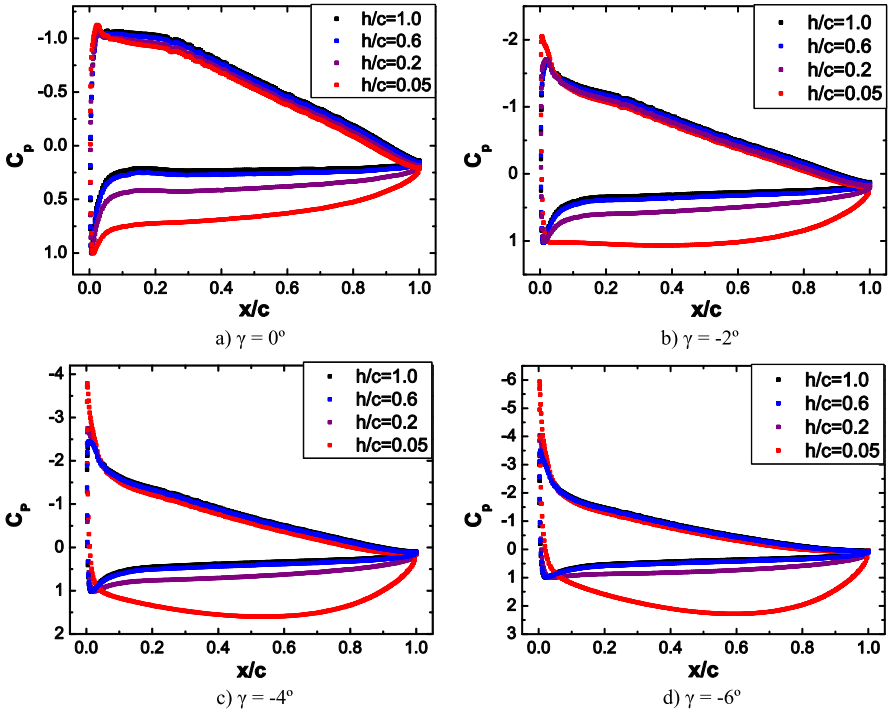

Fig. 9. Pressure coefficient for NACA 4412 airfoil with $\theta = 4°$ at different sink rates and ride heights.

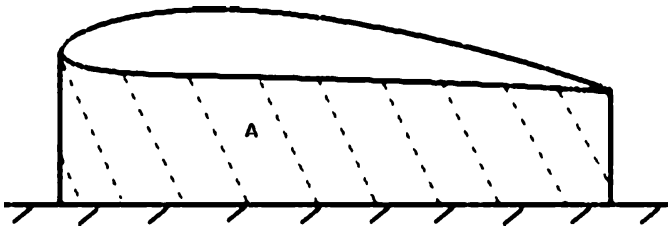

Fig. 10. Sketch of area A between the airfoil and the ground.

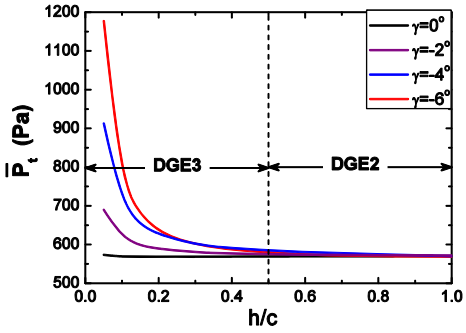

Fig. 11. Variation of the averaged total pressure in area A of Fig. 10 with ride height at $\theta = 4°$.

note is that the increments in the suction peak and lower surface pressure are enhanced with increasing sink rate.

In many aerodynamic problems where one is primarily interested in lift, the work done by external forces such as gravity and viscous forces is neglected. For incompressible flow, the C_p at stagnation point is 1. In this investigation, C_p is much larger than 1 on the pressure surface when h/c in DGE is very small; the explanation of this result is given below.

As shown later in Fig. 13, in DGE there exist two branches of airflow: uniform inflow from upstream and downwash flow due to the moving airfoil. Those two streams of airflow couple into one composite flow. In the unbounded flow field, the downwash flow moves freely; while in DGE, the downwash flow is blocked by the ground and moves towards the leading edge and trailing edge of the airfoil to escape. The channel between the lower surface of the airfoil and the ground becomes narrower with decreasing h/c, so the downwash flow does not have sufficient space to escape and therefore is compressed. As a result, the mechanical energy of the air increases, i.e. the airfoil does compression work on the fluid below it.

In order to analyze the compression work on the air done by the airfoil, we define an area A of the channel between the lower surface of the airfoil and the ground as shown in Fig. 10.

The total pressure p_t of an arbitrary point in A is defined as:

$$p_t = \frac{1}{2}\rho V^2 + p \tag{4}$$

Averaged total pressure $\overline{p_t}$ of the fluid in A with h/c and γ is defined as:

$$\overline{p_t}(h/c, \gamma) = \frac{1}{A}\iint_A p_t dA \tag{5}$$

Fig. 11 shows that $\overline{p_t}$ of the air in A remains constant at different ride heights in SGE. In DGE 2, the total pressure increases slightly with decrease in h/c indicating that the airfoil begins to compress the air, but the compression effect is very weak. In DGE 3, the total pressure increases rapidly and gets larger with larger sink rate indicating that the compression effect is a significant factor now.

Neglecting viscosity and gravity, the energy conservation equation for the air below the airfoil in DGE can be approximately written as:

$$p_\infty + \frac{1}{2}\rho V_\infty^2 + W(h/c, \gamma) = \frac{1}{2}\rho V^2 + p \tag{6}$$

where $W(h/c, \gamma)$ is the compression work done by the airfoil and is a function of both h/c and γ. When h/c decreases, the moving airfoil does more work. When the sink rate increases, the compression ratio of the air increases resulting in larger compression forces and more compression work.

Substituting Eq. (6) into Eq. (3), the C_p on the lower surface of the airfoil in DGE can be obtained as:

$$C_p = \frac{p - p_\infty}{\frac{1}{2}\rho V_\infty^2} = 1 - \left(\frac{V}{V_\infty}\right)^2 + \frac{W(h/c, \gamma)}{\frac{1}{2}\rho V_\infty^2} \tag{7}$$

From Eq. (7), it can be seen that C_p on the lower surface of the airfoil in DGE is probably greater than 1. This is because the air below the airfoil is subjected to compression and thus its mechanical energy increases, resulting in an increase in static pressure.

Fig. 12 shows C_p on the airfoil with $\theta = 4°$ and $\gamma = -4°$ in DGE; it is compared with C_p on the airfoil at $\alpha = 8°$ in SGE. Pressure coefficients in DGE and SGE agree quite well at $h/c = 0.6$; this figure clearly demonstrates that the major factors that govern the flow in DGE 2 are the combined incidence effect and SGE. At $h/c = 0.2$, the pressure on the lower surface of the airfoil and the suction peak in DGE are significantly larger than those in SGE. As h/c decreases, for example at $h/c = 0.05$, the difference becomes much greater, which indicates that in DGE 3 compression work done by the airfoil is a major factor in addition to the former two factors.

4.3. Flow field analysis and discussion

Fig. 13 depicts the streamlines and pressure contours around NACA 4412 airfoil in unbounded flow field and in ground effect at $\theta = 4°$. All streamlines are created using the velocity that is relative to the initial position of the airfoil.

Fig. 13a) shows a static airfoil in uniform inflow. Compared to the unbounded flow field, the streamlines below the airfoil in SGE are straighter, the stream tubes are broader, and thus the flow velocity is slower and the pressure is larger. This is the reason that the lift in SGE is larger than that in the unbounded flow field.

In Fig. 13b), there is no inflow from upstream and the airfoil descends at a constant velocity. The airfoil drives the air below it and produces a downwash flow, simultaneously forming the leading-edge and trailing-edge vortices. In the unbounded flow field, the downwash flow can develop freely and is vertically directed. While in DGE, there is no sufficient space for the downwash flow to develop and therefore the flow is compressed greatly. As a result, the pressure increases dramatically. Furthermore, the downwash flow is separated into two streams to escape from the leading-edge and trailing-edge. This escaping airflow moves almost parallel to the ground, therefore the distance between the cores of two vortices and the upper surface of the airfoil increases.

In Fig. 13c), there is uniform inflow from upstream and the airfoil descends at a constant velocity. In this case, the upstream inflow and the downwash flow streams couple into one composite flow. Because of the velocity reference point selected here, there is only a saddle point in the flow field instead of the stagnation point on the airfoil surface. The composite flow is divided into four streams by the saddle point. The inflow from upstream is separated into an upward stream and a downward stream respectively passing from the upper and lower surfaces of the airfoil. The downwash flow is separated into a forward flow and a backward

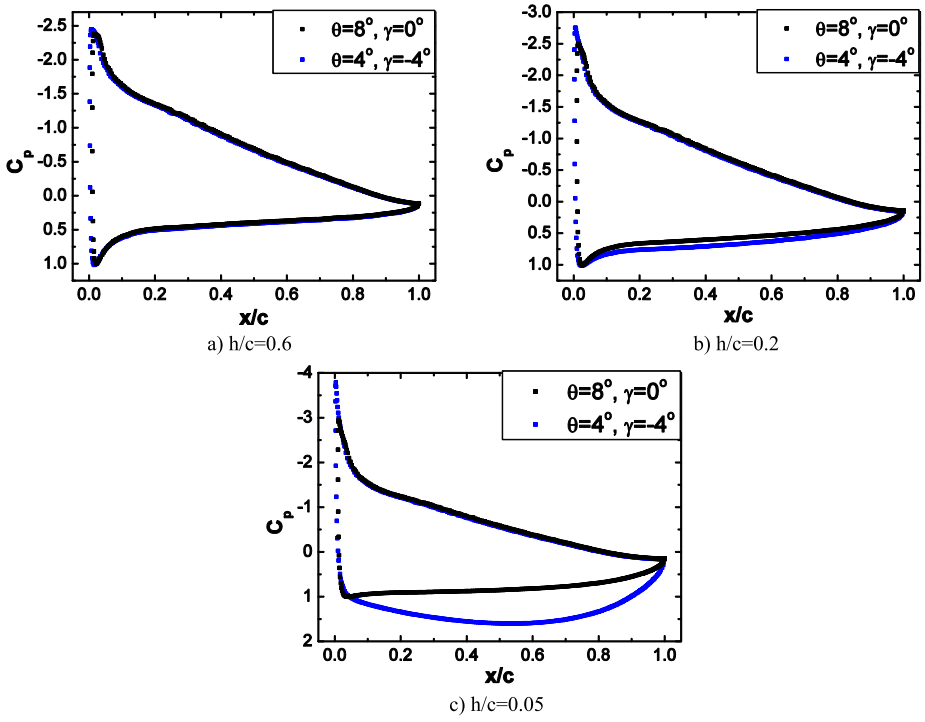

Fig. 12. Comparison of pressure coefficients of NACA 4412 airfoil for DGE and SGE at various ride heights.

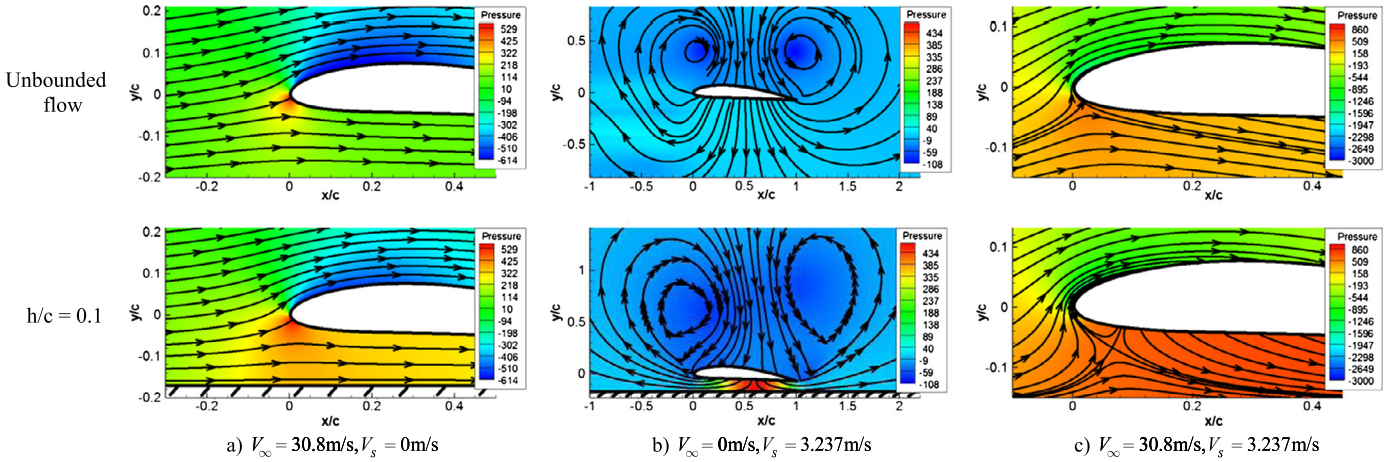

Fig. 13. Streamlines and pressure contours around NACA 4412 at $\theta = 4°$.

flow respectively escaping from the leading edge and the trailing edge.

Fig. 14 depicts the streamlines and pressure contours around NACA 4412 airfoil in DGE at $\theta = 4°$ and $\gamma = -4°$.

In the unbounded flow field (DGE 1), the saddle point is very close to the leading edge of the lower surface of the airfoil. It is because the airfoil does not do compression work in this region and the static pressure of the air below the airfoil is so small that it cannot resist the upstream inflow. As a result, almost all the downwash flow passes through the trailing edge.

In DGE 2 (see Fig. 14a)), the position of the saddle point is nearly the same as that in DGE 1 since the compression work is still very small in DGE 2; the static pressure below the airfoil does not increase significantly, therefore it cannot resist the upstream inflow.

In DGE 3 (see Figs. 14b)–14d)), the saddle point moves toward the trailing edge and the ground when h/c decreases. It is important to note here that the moving velocity of the saddle point increases with decrease in h/c. For example, at $h/c = 0.05$, the saddle point is almost on the ground. This is because the compression work done by the airfoil increases significantly as the airfoil moves closer to the ground resulting in large increase in static pressure of the air below the airfoil. This high pressure air can finally resist the upstream inflow, forcing more upstream inflow to go over the upper surface. At the same time, more downwash flow is diverted from the leading edge. At $h/c = 0.05$, the increase of static pressure due to the compression work is so large that nearly all the upstream inflow is diverted from the upper surface. The channel below the lower surface is primarily occupied by the downwash flow.

It can be concluded from the above analysis that in DGE, more upstream inflow and downwash flow are forced to go over the upper surface of the airfoil with the reduced ride height. As a result, the fluid velocity near the leading edge increases including the suction peak (see Fig. 9 and Fig. 12).

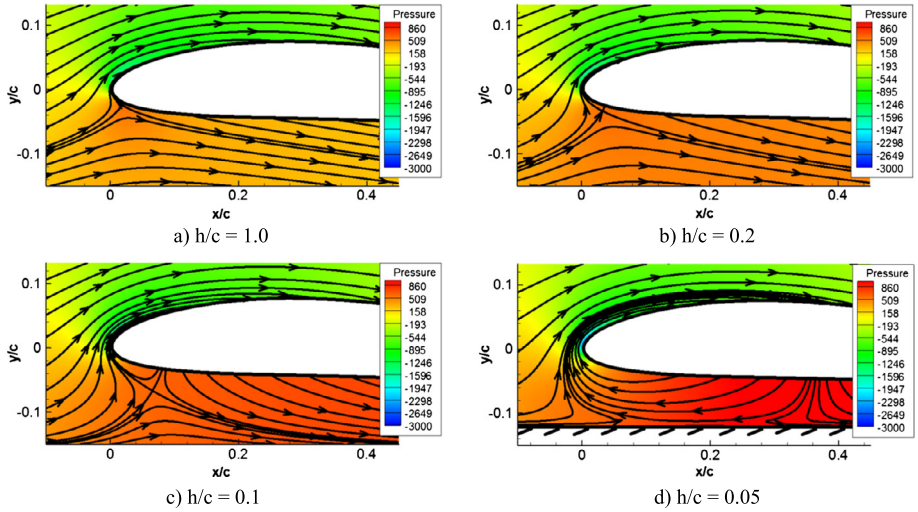

Fig. 14. Streamlines and pressure distributions around NACA 4412 airfoil at $\theta = 4^\circ$ and $\gamma = -4^\circ$ for various h/c.

5. Conclusions

CFD simulations are employed to study the flow field and the aerodynamic properties of a NACA 4412 airfoil in DGE. First, the accuracy of the numerical method is validated by computing the flow past Tyrrell-026 airfoil and comparing the results with experimental data. Then, the flow fields around the airfoil in SGE and DGE (descending at different sink rates towards the ground) are simulated. From the analysis of the flow properties and aerodynamic forces, it is found that DGE can be divided into three regions based on the ride height.

1) DGE 1 ($h/c > 1.0$): the lift in DGE is equal to that in SGE for the same angle of attack and does not change with the ride height. It is because DGE 1 is out of ground effect and the main physics that governs the flow is the incidence effect induced by the sinking movement.
2) DGE 2 ($0.5 < h/c < 1.0$): the lift in DGE is almost equal to that in SGE for the same angle of attack and increases with decreasing ride height. It is because of increase in pressure on the lower surface of the airfoil. The main factor that governs the flow is the coupling of SGE and the incidence effect.
3) DGE 3 ($h/c < 0.5$): when the ride height decreases significantly, the lift in DGE gradually becomes larger than that in SGE for the same angle of attack. The lift difference between DGE and SGE becomes more significant with larger sink rate. Furthermore, in addition to SGE and incidence effect, compression work effect becomes an important factor that governs the flow. The air below the airfoil does not have sufficient space to escape as the airfoil moves towards the ground; thus this air is compressed and the static pressure increases significantly, resulting in an increase in lift. Compression work effect becomes quite apparent at relatively small ride height.

Furthermore, in the study of chord dominated DGE during landing, a dynamic case can be treated as the static case with the same angle of attack in the following two circumstances – (1) the sink rate is very small and (2) the relative ride height is larger than 0.5 ($h/c > 0.5$) even if the sink rate is very large.

Conflict of interest statement

There is no conflict of interest with any person or entity concerning the research reported in this paper.

Acknowledgements

This work was partially supported by the National Natural Science Foundation of China (No. 11302015) and the State Scholarship Fund of China (No. 201203070193).

References

[1] M.R. Ahmed, T. Takasaki, Y. Kohama, Aerodynamics of a NACA 4412 airfoil in ground effect, AIAA J. 45 (2007) 37–47.
[2] P.A. Baker, W.G. Schweikhard, W.R. Young, Flight evaluation of ground effect on several low-aspect-ratio airplanes, NASA-TN-D-6053, 1970.
[3] Y.S. Chen, W.G. Schweikhard, Dynamic ground effects on a two-dimensional flat-plate, J. Aircr. 22 (1985) 638–640.
[4] S. Corda, M.T. Stephenson, F.W. Burcham, R.E. Curry, Dynamic ground effects flight test of an F-15 aircraft, NASA-TM-4604, 1994.
[5] R.E. Curry, Dynamic ground effect for a cranked arrow wing aircraft, NASA-TM-4799, 1997.
[6] G. Doig, T.J. Barber, Considerations for numerical modeling of inverted wings in ground effect, AIAA J. 49 (2011) 2330–2333.
[7] S.H. Lee, J. Lee, Optimization of three-dimensional wings in ground effect using multiobjective genetic algorithm, J. Aircr. 48 (2011) 1633–1645.
[8] S. Mahon, X. Zhang, Computational analysis of pressure and wake characteristics of an aerofoil in ground effect, J. Fluids Eng. – Trans. ASME 127 (2005) 290–298.
[9] T. Matsuzaki, S. Yoshioka, T. Kato, Y. Kohama, Unsteady aerodynamic characteristics of wings in ground effect, in: Proceedings of the 40th JAXA Workshop on Investigation and Control of Boundary-Layer Transition, 2008, pp. 53–56.
[10] J. Molina, X. Zhang, Aerodynamics of a heaving airfoil in ground effect, AIAA J. 49 (2011) 1168–1179.
[11] A.O. Nuhait, M.F. Zedan, Numerical simulation of unsteady flow induced by a flat plate moving near ground, J. Aircr. 30 (1993) 611–617.
[12] X.G. Qin, Numerical Simulation of High Lift Device in Ground Effect, Beijing University of Aeronautics and Astronautics, Beijing, 2010.
[13] Q.L. Qu, X. Jia, W. Wang, P.Q. Liu, R.K. Agarwal, Numerical simulation of the flowfield of an airfoil in dynamic ground effect, J. Aircr. (2014), http://dx.doi.org/10.2514/1.c032452, in press.
[14] L.S. Rolls, D.G. König, Flight measured ground effect on a low-aspect-ratio Ogee wing including a comparison with wind-tunnel results, NASA-TN-D-3431, 1966.
[15] K.V. Rozhdestvensky, Aerodynamics of a Lifting System in Extreme Ground Effect, Springer, 2000.
[16] K.V. Rozhdestvensky, Wing-in-ground effect vehicles, Prog. Aerosp. Sci. 42 (2006) 211–283.
[17] D.F. Wang, C. Dai, Experimental research on the aerodynamics of a symmetrical airfoil near free surface, J. Hydrodyn. (2010) 703–710.
[18] Z.G. Yang, W. Yang, Complex flow for wing-in-ground effect craft with power augmented ram engine in cruise, Chin. J. Aeronaut. 23 (2010) 1–8.
[19] L. Yun, A. Bliault, J. Doo, WIG Craft and Ekranoplan: Ground Effect Craft Technology, Springer, 2010.
[20] X. Zhang, J. Zerihan, Edge vortices of a double-element wing in ground effect, J. Aircr. 41 (2004) 1127–1137.